

Determination of Sapphire Off-Cut and Its Influence on the Morphology and Local Defect Distribution in Epitaxially Laterally Overgrown AlN for Optically Pumped UVC Lasers

Johannes Enslin,* Arne Knauer, Anna Mogilatenko, Frank Mehnke, Martin Martens, Christian Kuhn, Tim Wernicke, Markus Weyers, and Michael Kneissl

Herein, a systematic study of the morphology and local defect distribution in epitaxially laterally overgrown (ELO) AlN on *c*-plane sapphire substrates with different off-cut angles ranging from 0.08° to 0.23° is presented. Precise measurements of the off-cut angle α , using a combination of optical alignment and X-ray diffraction with an accuracy of $\pm 5^\circ$ for the off-cut direction and $\pm 0.015^\circ$ for the off-cut angle, are carried out. For ELO AlN growth, a transition from step flow growth at $\alpha < 0.14^\circ$ with height undulations on the surface to step bunching with step heights up to 20 nm for $\alpha > 0.14^\circ$ is observed. Furthermore, the terraces of the step-bunched surface exhibit curved steps. An analysis of the local defect distribution by scanning transmission electron microscopy and a comparison with atomic force microscopy reveal a bunching of defects in line with the ELO pattern and a roughening of step edges in highly defective regions. In addition, a reduction in the threshold excitation power density for optically pumped ultraviolet-C (UVC) lasers with smooth surface morphologies is observed.

These devices require high-quality layers in terms of dislocation density as well as smooth surface morphologies to reach high efficiencies, high output power levels, and, in the case of LDs, low-threshold power densities. The relatively high threading dislocation densities (TDDs) of the AlN template layers used for AlGaN growth^[5] limit the internal quantum efficiency of optical devices.^[6] Epitaxially laterally overgrown (ELO) AlN/sapphire^[7] is one method for the effective TDD reduction on *c*-plane sapphire substrates. This ELO process allows a TDD reduction down to $5 \times 10^8 \text{ cm}^{-2}$.^[8,9]

In this article, we present the systematic variation of the off-cut angle of (0001)-oriented sapphire substrates and its impact on the surface morphology and the local defect distribution of ELO AlN/sapphire


1. Introduction

Light-emitting diodes (LEDs) and laser diodes (LDs) emitting in the ultraviolet-C spectral region between 200 and 280 nm have a wide range of applications such as water purification,^[1] disinfection of surfaces, gas sensing,^[2,3] and medical diagnostics.^[4]

templates. In a previous study, we compared ELO AlN/sapphire templates on sapphire wafers with nominal off-cut angles of $0.1^\circ \pm 0.1^\circ$ and $0.2^\circ \pm 0.1^\circ$. Off-cut angles of $0.2^\circ \pm 0.1^\circ$ resulted in the formation of macrosteps with heights of several nanometers.^[10] Here, the off-cut angle was determined by precise X-ray diffraction (XRD) measurements combined with an optical alignment. Subsequently, the wafers were processed and overgrown to obtain ELO AlN/sapphire templates. Their surface morphology as well as their defect distribution was investigated by atomic force microscopy (AFM) and scanning transmission electron microscopy (STEM), respectively. Furthermore, laser heterostructures were grown with an emission wavelength of 270–275 nm on these templates to investigate the influence of the template morphology on the performance of optically pumped devices.

J. Enslin, Dr. F. Mehnke, Dr. M. Martens, C. Kuhn, Dr. T. Wernicke, Prof. M. Kneissl
Institut für Festkörperphysik
Technische Universität Berlin
Hardenbergstr. 36, EW 6-1, 10623 Berlin, Germany
E-mail: johannes.enslin@physik.tu-berlin.de

Dr. A. Knauer, Dr. A. Mogilatenko, Prof. M. Weyers, Prof. M. Kneissl
Ferdinand-Braun-Institut
Leibniz-Institut für Höchstfrequenztechnik
Gustav-Kirchhoff-Str. 4, 12489 Berlin, Germany

 The ORCID identification number(s) for the author(s) of this article can be found under <https://doi.org/10.1002/pssa.201900682>.

© 2019 The Authors. Published by WILEY-VCH Verlag GmbH & Co. KGaA, Weinheim. This is an open access article under the terms of the Creative Commons Attribution License, which permits use, distribution and reproduction in any medium, provided the original work is properly cited.

DOI: 10.1002/pssa.201900682

2. Determination of Sapphire Off-Cut

Since the transition from step flow growth to step bunching for ELO AlN/sapphire occurs at very small off-cut angles between 0.1° and 0.2° ,^[10] a highly accurate determination of the substrate off-cut is necessary to determine the critical angle for this transition. Thus, precise off-cut measurements were carried out using a combination of an optical alignment of the wafer and

XRD reciprocal space maps (φ/ω). This technique is similar to the one described by Halliwell and Chua^[11] extended by an additional alignment step of the wafer. Using this alignment, the surface normal of the sapphire wafer can be adjusted parallel to the rotation axis of the diffractometer. **Figure 1** shows the setup for the off-cut determination.^[12] The wafer is mounted onto a tiltable sample holder in a Philips X'Pert MRD Pro X-ray diffractometer. The X-ray beam is directed onto the sample under the angle ω . The cradle can either be rotated around its rotation axis (φ -angle) or tilted perpendicular to the plane of the beam (χ -angle).^[13] A collimated red laser beam is directed at the center of the sample holder—corresponding to the rotation axis position—and is reflected by the sapphire surface. Using two mirrors, the reflected beam is guided over a distance of 15 m to a screen. Typically an inplane rotation around the rotation axis of the diffractometer results in a precession of the laser spot on the screen due to the tilt between the surface normal and the goniometer axis. By tilting the sample holder independently from the goniometer ($\omega/\varphi/\chi$), the precession radius was minimized, which corresponds to an adjustment of the surface normal parallel to the rotation axis of the diffractometer. The error for the following measurements was estimated by correlating the radius of the residual precession to a shift in the ω -angle of the goniometer. The error was estimated for every single measurement and ranges from $\pm 0.007^\circ$ to $\pm 0.015^\circ$.

After the alignment of the surface normal to the goniometer rotation axis, a map in ω and φ of the (0006) reflection of sapphire was acquired (**Figure 2**). A rotation of the wafer variation of φ -angle results in a variation of the peak position in ω -direction, as the lattice planes are tilted according to the off-cut angle. The location of each peak in the ω scans was extracted, and the resulting peak position $\omega_{\max}(\varphi)$ was fitted with a sine function (solid blue line). The amplitude of the sine curve corresponds directly to the off-cut angle α marked in red. As shown in **Figure 2** by gray lines, a minimum of the sine function at $\varphi = 0$ would correspond to a wafer with a pure off-cut into the m -direction of sapphire (considering the orientation of the wafer in relation to the goniometer, shown in **Figure 2**). A shift of the minimum of the sine function to positive or negative φ -angles indicates a shift of the direction of the off-cut toward the a -direction of sapphire ($\varphi = 90^\circ$ for pure off-cut toward the a -direction of sapphire), which is the case for the measured off-cut in **Figure 2** (black hexagons).

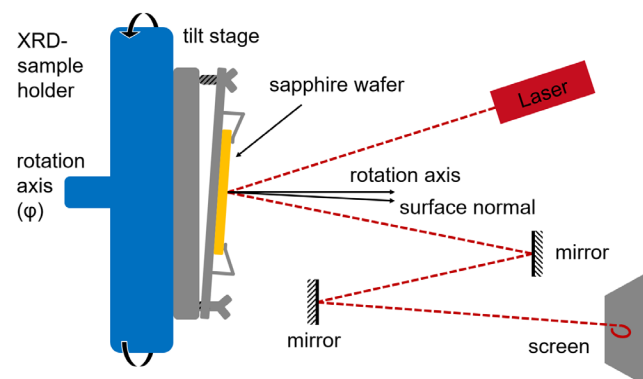


Figure 1. Experimental setup to align the surface normal of the sapphire wafer parallel to the rotation axis (φ) of the XRD sample holder.

The position of the flat is used to determine the off-cut direction. The misalignment of the flat given by the manufacturer is $\pm 0.2^\circ$ in reference to the $[11\bar{2}0]$ direction of sapphire, which is negligible in comparison with the estimated error due to the manual alignment of the wafer on the goniometer, which is estimated to be $\pm 5^\circ$. In case a higher precision is required, the measurement can be extended by an asymmetric φ -scan to correlate the crystal axis to the sample holder; however, this was not performed for the measured wafers. The off-cut angle α can be split into the component in the sapphire m -direction (α_m) by calculating the difference in ω for $\varphi = 0^\circ$ and $\varphi = \pm 180^\circ$ (see **Figure 2**). Accordingly, the sapphire a -direction component (α_a) can be calculated by evaluating the ω -angle at $\varphi = -90^\circ$ and $\varphi = 90^\circ$. The correlation between the off-cut α and its components α_a and α_m is given by: $\alpha = \sqrt{\alpha_a^2 + \alpha_m^2}$. Two batches of c -orientated sapphire wafers with nominal off-cut angles of $0.1^\circ \pm 0.1^\circ$ and $0.2^\circ \pm 0.1^\circ$ toward the sapphire m -direction were examined. For wafers with a nominal off-cut angle of $0.1^\circ \pm 0.1^\circ$, we observed variations from 0.08° to 0.12° and for wafers with a nominal off-cut angle of $0.2^\circ \pm 0.1^\circ$, values between 0.16° and 0.23° were observed. Although, the specifications given by the wafer supplier are satisfied, there is a certain variety within each batch of wafers. To cover a broad range of off-cut angles, we selected eight wafers with off-cut angles varying from 0.08° to $0.1^\circ \pm 0.23^\circ$ for further investigations (see **Figure 3**, open symbols).

3. ELO AlN/Sapphire Morphology and Defects

3.1. Experimental Procedure

After the determination of the off-cut angles, the sapphire wafers were overgrown with a $0.5 \mu\text{m}$ -thick AlN layer in an Aixtron 2400-G3 planetary reactor with standard precursors.^[14] Subsequently, these templates were patterned with stripes along the $[10\bar{1}0]$ direction of AlN ($[2\bar{1}\bar{1}0]$ direction of sapphire) and overgrown with $5.8 \mu\text{m}$ ELO AlN, as described in the study by

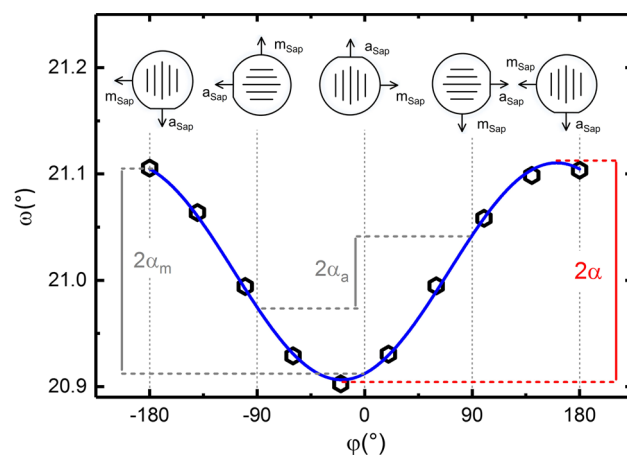


Figure 2. Peak positions of an ω - φ -XRD map of a sapphire wafer near the (0006) reflection indicating the off-cut angle α and the components in a - and m -directions (α_a and α_m). The direction in reference to the flat is illustrated in the upper half of the image. The stripes drawn on the wafer schematic depict the direction of the processed ELO trenches.

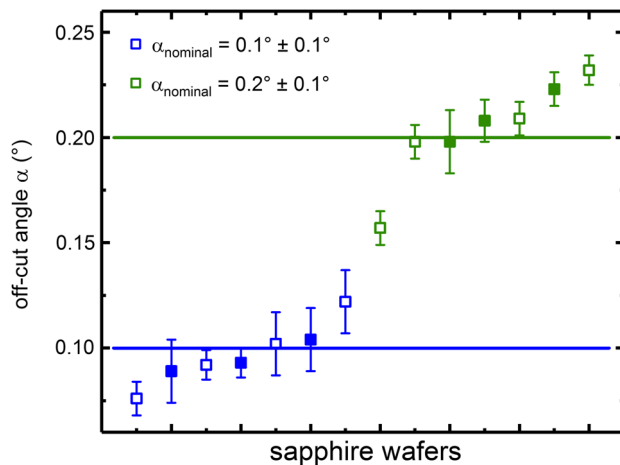


Figure 3. Off-cut angles α of two batches of sapphire wafers with nominal off-cut angles of $0.1^\circ \pm 0.1^\circ$ (blue) and $0.2^\circ \pm 0.1^\circ$ (green). Open symbols mark the selected wafers for further analysis.

Knauer et al.^[10] The morphology and local defect distribution of these ELO AlN/sapphire templates were investigated using AFM and STEM.

3.2. Surface Morphology of ELO AlN/Sapphire

In **Figure 4**, AFM images are shown, presenting the surface morphology of ELO AlN grown on sapphire wafers with different off-cut angles to the sapphire *m*-direction. For off-cut angles between 0.08° and 0.12° , the images show a wavelike surface morphology with monoatomic steps and an overall undulation with a height difference between the lowest and the highest point on the surface ranging from 3 to 5 nm. For higher off-cut angles ($0.16^\circ - 0.23^\circ$), the AlN surfaces exhibit macrosteps with increasing heights from 14 nm at $\alpha = 0.16^\circ$ to 21 nm at $\alpha > 0.20^\circ$. The periodicity of the wavelike surface features as well as the periodicity of the macrosteps for high off-cut angles corresponds to the periodicity of the underlying ELO pattern of $3.5 \mu\text{m}$. In addition, AFM images give insight into the roughness of the grown samples. The root mean square (RMS) roughness was evaluated on a $20 \mu\text{m} \times 20 \mu\text{m}$ scale and is shown in **Figure 4**. Templates with off-cut angles between 0.08° and 0.12° exhibit rather smooth surfaces with low and constant RMS values around 1.5 nm. On the contrary, templates with off-cut angles between 0.16° and 0.23° exhibit RMS values increasing from 3.5 to 5.3 nm with increasing off-cut angle. The surface morphologies for this wide

range of off-cut angles were investigated and showed a transition from a wavelike surface morphology to a surface with macrosteps at a critical angle of $\alpha = 0.14^\circ \pm 0.02^\circ$ for this growth parameter regime.^[14] This can be explained by the fact that the height of the surface steps appearing at coalescence positions of two neighboring ELO stripes increased with increasing off-cut angle. The high steps cannot be planarized anymore with further overgrowth to obtain a smooth surface for $\alpha > 0.14^\circ$. Thus, the surface steps are preserved during subsequent growth, which results in step bunching at the surface. Detailed studies would be necessary to completely understand the transition from smooth morphologies to step bunching.

A closer look at the samples exhibiting step bunching reveals the surface morphology of the macroterrace (area between macrosteps). In **Figure 5a**, a single macrostep was selected, and the monoatomic step edges observed on the macroterrace were marked in green. The terrace exhibits a convex bow with the lowest points close to the macrostep edge. Furthermore, the monoatomic steps are curved. The normal to the curve of the step (green lines in **Figure 5a**) in the middle between the macrosteps points into the *m*-direction of AlN $[10\bar{1}0]$ ($[2\bar{1}\bar{1}0]$ direction of sapphire) (i.e., the step flow takes place along the macrosteps). **Figure 5b** shows step flow growth on the highest point of the convex terrace (purple area) with large terrace widths between the steps of over 400 nm. In contrast, **Figure 5c** shows monoatomic steps—close to the macroterrace edge—running along the AlN *a*-direction $[1\bar{2}10]$ ($[10\bar{1}0]$ direction of sapphire) (i.e., the step flow takes place across the macroterrace) with terrace width between the steps of less than 100 nm. The off-cut toward the *m*-direction $[10\bar{1}0]$ of sapphire ($[1\bar{2}10]$ direction of AlN) on the terrace is quite small due to a compensation through the stepped surface, and thus the fraction of the off-cut toward the sapphire *a*-direction $[2\bar{1}\bar{1}0]$ ($[10\bar{1}0]$ direction of AlN, parallel to macrosteps) dictates the step flow direction. The convex shape of the terrace could be explained by diffusion of adatoms over the edge of the macrostep, leading to a reduced growth rate close to the macrostep.

3.3. Local Defect Distribution in ELO AlN/Sapphire

By conducting high-resolution AFM measurements, it is possible to observe surface pits which are most likely caused by threading dislocations. Tarsa et al. found that the number and type of surface pits observed by AFM in GaN films fit very well to the defect density determined by transmission electron microscopy (TEM).^[15] To visualize single defects, AFM images were acquired, and a polynomial background was subtracted from the recorded data to flatten the image. The processed AFM

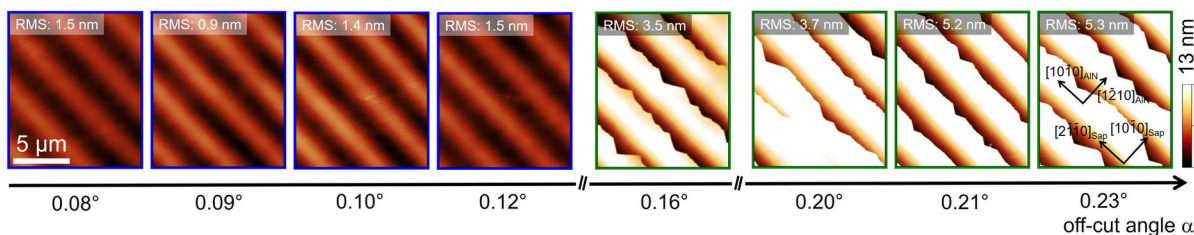


Figure 4. AFM micrographs of the ELO AlN/sapphire surface for increasing sapphire off-cut angles from 0.08° to 0.12° with wavelike surface morphology and from 0.16° to 0.23° with step bunching and corresponding RMS roughness measured on a $20 \mu\text{m} \times 20 \mu\text{m}$ area.

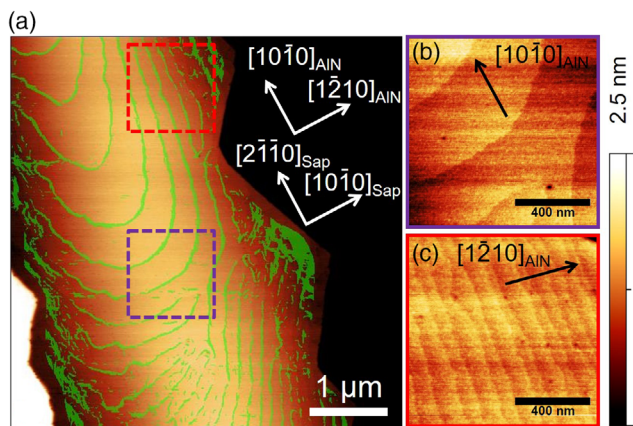


Figure 5. a) AFM images of one convex macrostep terrace grown on a sapphire wafer with an off-cut angle of 0.16° , b) exhibiting wide monoatomic steps (image taken from the area marked with a purple square in (a), and c) small terrace widths between the steps (this image is taken from a similar area of the macrostep terrace as marked in (a) in red).

images are shown in **Figure 6a,b**), and the local defect densities were determined. In **Figure 5a**, for example, dislocations with a screw component can be identified by two monolayer steps originating from the pits, as marked by red circles; furthermore,

areas close to the macrostep exhibit a high defect density of about $1 \times 10^{10} \text{ cm}^{-2}$. This value corresponds very well to the defect density of planar AlN/sapphire templates.^[10] Furthermore, there is a $1.5 \mu\text{m}$ -wide region exhibiting a reduced defect density of $1 \times 10^9 \text{ cm}^{-2}$. As shown in the cross-section annular dark-field (ADF) STEM image (see the study by Mehnke^[12]) in **Figure 6c**, the pattern of a $1.5 \mu\text{m}$ -wide defect-reduced region above the trenches followed by a $2 \mu\text{m}$ -wide defect-rich region is consistent with the AFM image. The mean defect density obtained by STEM correlates well with the one extracted from the AFM images as well as defect densities calculated from XRD rocking curves^[13] of the (0002) and (3032) reflections which are all in the range of $6 \times 10^9 \text{ cm}^{-2}$. The measurement geometry was selected such that the incoming X-ray beam was parallel to the direction of the ELO trenches (in AlN [1010] direction) to avoid additional peak broadening due to wing tilt.^[16] **Figure 6b** shows the defects on the surface for a template grown on a sapphire wafer with an off-cut angle of 0.12° . A $2 \mu\text{m}$ -wide area proceeding from the upper left corner of the image to the lower right corner exhibits a high density of defects. Furthermore, the growth fronts of the monoatomic steps are rougher in this area compared with the remaining part of the image due to impediment of the step motion by defects. The defect densities in the two areas are almost identical to those of samples with high off-cut angles.

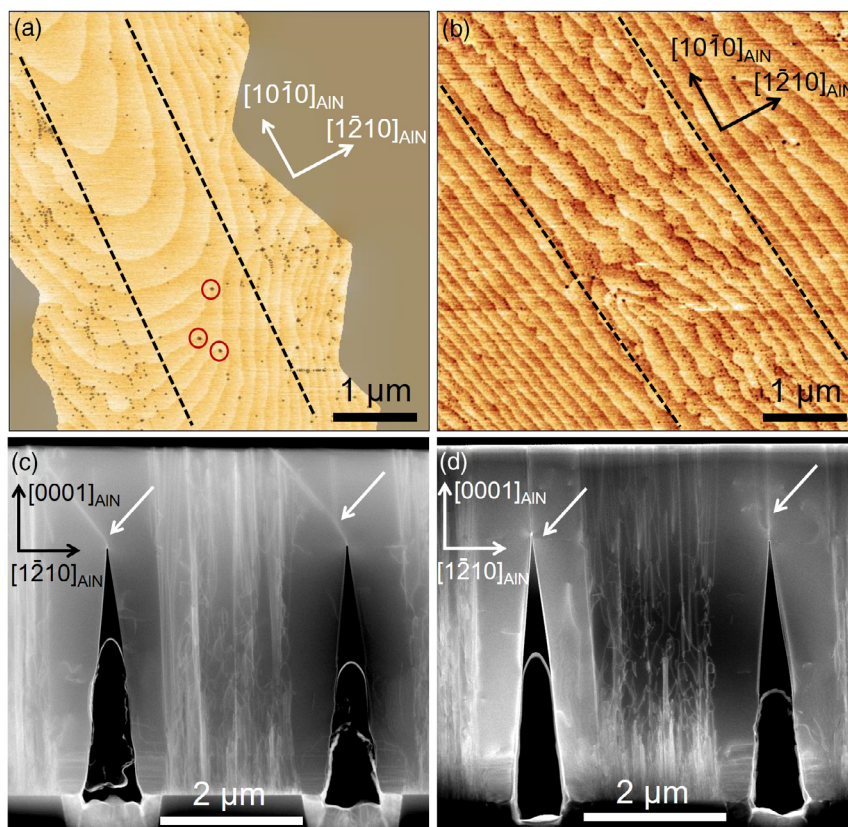


Figure 6. AFM images flattened by subtraction of a polynomial background of an ELO AlN/sapphire surface with a) stepbunches and b) a wavelike surface morphology illustrating defect-rich regions between the dashed lines and the macrostep edge and between the dashed lines, respectively. Cross-section ADF STEM images showing the defect distribution in ELO AlN/sapphire with off-cut angles of c) $\alpha > 0.14^\circ$ and d) $\alpha < 0.14^\circ$. White arrows indicate coalescence boundaries between two wing regions.

A comparison with ADF STEM images (Figure 6d) reveals the same geometrical pattern and defect distribution as the AFM investigations. ELO AlN/sapphire samples with high off-cut angles show an inclined grain boundary, whereas samples grown on substrates with low off-cut angles exhibit a vertical grain boundary originating from the coalescence region. The inclination of threading dislocations for higher off-cuts is caused by formation of the macrostep at the coalescence position and its lateral propagation during further growth, which is already described in the study by Knauer et al.^[10] Contrary to that, samples with low off-cut angles exhibit no macrosteps boundaries, and the correlation between the underlying ELO pattern and the surface undulations is fixed. Therefore, the conclusion can be drawn that the off-cut angles in the investigated ELO AlN/sapphire templates have no significant influence on the defect distribution but on the surface morphology at a given thickness of 2 μm after coalescence of the investigated templates. It should be noted that a thicker ELO AlN layer ($>6 \mu\text{m}$) for templates with high off-cut angles and inclined grain boundaries can result in a collection and partial annihilation of dislocations.^[9]

4. Optically Pumped Laser Structures

4.1. Experimental Procedure

Finally, optically pumped laser structures consisting of AlGaIn multiple quantum wells emitting between 270 and 275 nm embedded in $\text{Al}_{0.7}\text{Ga}_{0.3}\text{N}$ waveguides and an AlGaIn cladding layer^[17] were grown on top of ELO AlN/sapphire templates. Excitation power-dependent photoluminescence (PL) measurements were carried out on laser bars with cleaved facets^[18] in stripe geometry using a 193 nm ArF laser as the optical excitation source.^[17] Modal losses of the grown structures were determined based on optical gain spectra obtained by the variable stripe length method.^[19]

4.2. Off-Cut Influence on Laser Threshold

The net gain obtained from the variable stripe length method for both structures is shown in Figure 7a. The structure exhibiting step bunching shows internal losses, increased by a factor of five,

in comparison with the structure without step bunching. This results in a drastically decreased net gain. The integrated PL intensity collected from the facet as a function of the excitation power density for both structures is shown in Figure 7b. Both heterostructures exhibit lasing between 270 and 275 nm as the power-dependent PL intensity shows a threshold behavior in combination with spectral narrowing (not shown here).^[20] The laser structure on ELO AlN/sapphire with a smooth surface morphology exhibits lasing at a threshold power density of 1.7 MW cm^{-2} . This value is increased to 2.8 MW cm^{-2} for a laser structure grown on an ELO AlN/sapphire template exhibiting step bunching. This increase in threshold power density could be attributed to optical scattering losses within the waveguide due to 15–20 nm-high macrosteps. In addition, a stronger Ga incorporation at the macrostep edge^[8] can result in an increased modal loss due to absorption in Ga-rich regions. Considering this, avoiding macrosteps is crucial to achieve low laser thresholds. Therefore, the right choice of substrate off-cut for ELO AlN/sapphire needs to be considered. On the one hand, a sufficiently high substrate off-cut into the sapphire *m*-direction for ELO AlN/sapphire needs to be chosen to ensure coalescence and avoid nucleation of randomly distributed islands. On the other hand, the substrate off-cut chosen needs to be small enough, as shown in this study, to avoid macrosteps.

5. Conclusion

Using a combination of XRD and optical alignment of the sapphire surface, we measured the off-cut angles of *c*-plane sapphire wafers with a precision down to $\pm 0.015^\circ$. After AlN growth, processing, and overgrowth with ELO AlN, the surface morphology changes from a wavelike surface morphology to step bunching at a critical angle of $\alpha = 0.14^\circ \pm 0.02^\circ$ for the used AlN growth conditions. Macroterraces exhibit curved monoatomic steps. An analysis of the defect distribution on the surface by precise AFM and STEM measurements revealed an inhomogeneous distribution of the defects caused by ELO patterning with a similar overall defect density for both types of surface morphologies. The threshold power density for optically pumped lasing decreases drastically for laser structures emitting at 270 and

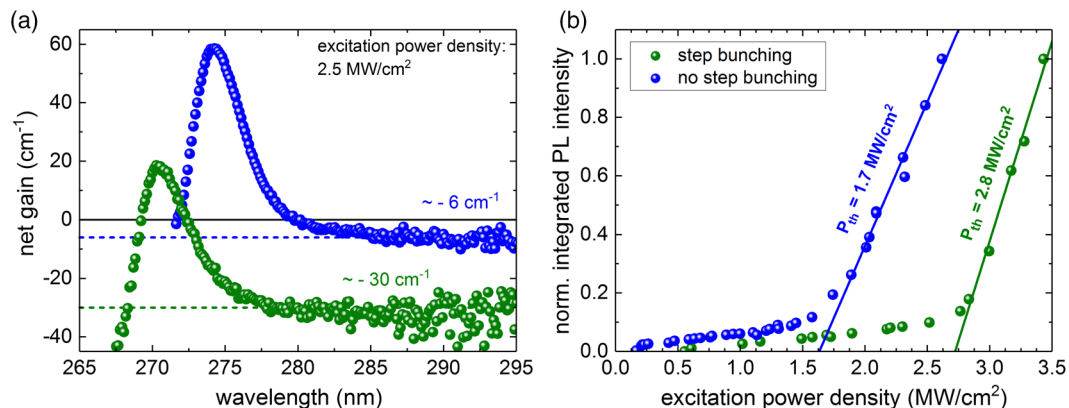


Figure 7. a) Net gain spectra for evaluation of internal losses and b) normalized integrated PL intensity versus excitation power density of an AlGaIn multiple quantum well laser structure grown on an ELO AlN/sapphire template without step bunching and with step bunching.

275 nm grown on surfaces exhibiting no macrosteps. These findings show that low laser thresholds of optically pumped laser structures can be achieved for *c*-plane sapphire wafers with smooth surface morphologies. For the presented ELO AlN/sapphire templates, this could be realized for off-cut angles $\alpha < 0.14^\circ$.

Acknowledgements

The authors would like to thank Tobias Meisch and Marian Calibe from University of Ulm for fruitful discussions. This work was partially supported by the Deutsche Forschungsgemeinschaft (DFG) within the Collaborative Research Centre 787 and the German Federal Ministry of Research and Education (BMBF) within the Advanced UV for Life initiative.

Conflict of Interest

The authors declare no conflict of interest.

Keywords

AlN, epitaxially laterally overgrown, off-cut, optically pumped lasers, sapphires, UVC

Received: August 21, 2019

Revised: October 18, 2019

Published online: November 12, 2019

-
- [1] S. Vilhunen, H. Särkkä, M. Sillanpää, *Environ. Sci. Pollut. Res.* **2009**, *16*, 439.
- [2] J. Hodgkinson, R. P. Tatam, *Meas. Sci. Technol.* **2013**, *24*, 012004.
- [3] F. Mehnke, M. Guttman, J. Enslin, C. Kuhn, C. Reich, J. Jordan, S. Kapanke, A. Knauer, M. Lapeyrade, U. Zeimer, H. Krüger, M. Rabe, S. Einfeldt, T. Wernicke, H. Ewald, M. Weyers, M. Kneissl, *IEEE J. Sel. Top. Quantum Electron.* **2017**, *23*, 29.
- [4] J. Hargis, J. Philip, T. J. Sobering, G. C. Tisone, J. S. Wagner, S. A. Young, R. J. Radloff, *Optical Instrumentation for Gas Emissions Monitoring and Atmospheric Measurements*, SPIE, McLean, VA **1995**.
- [5] M. Kneissl, J. Rass, *III-Nitride Ultraviolet Emitters: Technology and Applications*, Springer International Publishing, Schweiz **2015**.
- [6] S. Y. Karpov, Y. N. Makarov, *Appl. Phys. Lett.* **2002**, *81*, 4721.
- [7] V. Kueller, A. Knauer, C. Reich, A. Mogilatenko, M. Weyers, J. Stellmach, T. Wernicke, M. Kneissl, Z. Yang, C. Chua, N. Johnson, *IEEE Photonics Technol. Lett.* **2012**, *24*, 1603.
- [8] U. Zeimer, V. Kueller, A. Knauer, A. Mogilatenko, M. Weyers, M. Kneissl, *J. Crystal Growth* **2013**, *377*, 32.
- [9] A. Mogilatenko, V. Kueller, A. Knauer, J. Jeschke, U. Zeimer, M. Weyers, G. Traenkle, *J. Crystal Growth* **2014**, *402*, 222.
- [10] A. Knauer, A. Mogilatenko, S. Hagedorn, J. Enslin, T. Wernicke, M. Kneissl, M. Weyers, *Phys. Status Solidi (b)* **2016**, *253*, 809.
- [11] M. Halliwell, S. Chua, *J. Crystal Growth* **1998**, *192*, 456.
- [12] F. Mehnke, *Ph.D. Thesis*, Technische Universität (Berlin) **2017**.
- [13] M. A. Moram, M. E. Vickers, *Rep. Progress Phys.* **2009**, *72*, 036502.
- [14] O. Reentilae, F. Brunner, A. Knauer, A. Mogilatenko, W. Neumann, H. Protzmann, M. Heuken, M. Kneissl, M. Weyers, G. Traenkle, *J. Crystal Growth* **2008**, *310*, 4932.
- [15] E. J. Tarsa, B. Heying, X. H. Wu, P. Fini, S. P. DenBaars, J. S. Speck, *J. Appl. Phys.* **1997**, *82*, 5472.
- [16] D. Lübbert, T. Baumbach, P. Mikulk, P. Pernot, L. Helfen, R. Köhler, T. M. Katona, S. Keller, S. P. DenBaars, *J. Phys. D Appl. Phys.* **2005**, *38*, A50.
- [17] M. Martens, F. Mehnke, C. Kuhn, C. Reich, V. Kueller, A. Knauer, C. Netzel, C. Hartmann, J. Wollweber, J. Rass, T. Wernicke, M. Bickermann, M. Weyers, M. Kneissl, *IEEE Photonics Technol. Lett.* **2014**, *26*, 342.
- [18] J. van Look, S. Einfeldt, O. Kruger, V. Hoffmann, A. Knauer, M. Weyers, P. Vogt, M. Kneissl, *IEEE Photonics Technol. Lett.* **2010**, *22*, 416.
- [19] K. L. Shaklee, R. F. Leheny, *Appl. Phys. Lett.* **1971**, *18*, 475.
- [20] C. Kuhn, T. Simoneit, M. Martens, T. Markurt, J. Enslin, F. Mehnke, K. Bellmann, T. Schulz, M. Albrecht, T. Wernicke, M. Kneissl, *Phys. Status Solidi A* **2018**, *215*, 1800005.